

# Entanglement in finite quantum systems under twisted boundary conditions

Krissia Zawadzki and Luiz N. Oliveira

*Departamento de Física e Ciência Interdisciplinar,  
Instituto de Física de São Carlos, University of São Paulo,  
Caixa Postal 369, 13560-970 São Carlos, SP, Brazil*

Irene D'Amico

*Department of Physics, University of York, York, YO10 5DD, United Kingdom and  
Departamento de Física e Ciência Interdisciplinar,  
Instituto de Física de São Carlos, University of São Paulo,  
Caixa Postal 369, 13560-970 São Carlos, SP, Brazil*

In a recent publication, we have discussed the effects of boundary conditions in finite quantum systems and their connection with symmetries. Focusing on the one-dimensional Hubbard Hamiltonian under twisted boundary conditions, we have shown that properties, such as the ground-state and gap energies, converge faster to the thermodynamical limit ( $L \rightarrow \infty$ ) if a special torsion  $\Theta^*$  is adjusted to ensure particle-hole symmetry. Complementary to the previous research, the present paper extends our analysis to a key quantity for understanding correlations in many-body systems: the entanglement. Specifically, we investigate the average single-site entanglement  $\langle S_j \rangle$  as a function of the coupling  $U/t$  in Hubbard chains with up to  $L = 8$  sites and further examine the dependence of the per-site ground-state  $\epsilon_0$  on the torsion  $\Theta$  in different coupling regimes. We discuss the scaling of  $\epsilon_0$  and  $\langle S_j \rangle$  under  $\Theta^*$  and analyse their convergence to Bethe Ansatz solution of the infinite Hubbard Hamiltonian. Additionally, we describe the exact diagonalization procedure used in our numerical calculations and show analytical calculations for the case-study of a trimer.

## I. INTRODUCTION

The study of many-body phenomena has gained a new perspective with the recent collaboration between condensed matter (CM) and quantum information theory (QIT). Experimentally, technical advances fostered by QIT have allowed for a high control of nanoscale set-ups, turning into reality the possibility to simulate condensed matter models<sup>1-4</sup> and to measure their properties with single site resolution<sup>5-7</sup>. At a fundamental level, both communities have brought contributions to our understanding of quantum correlations. The concept of entanglement has become a key ingredient to investigate collective behavior arising from microscopic degrees of freedom, such as critical properties and quantum phase transitions<sup>8-10</sup>. In this context, a problem which has been receiving special attention deals with the conditions under which properties in the thermodynamical limit can be accurately assessed by means of finite systems<sup>11</sup>, in which boundary conditions play a crucial role in the system's symmetries. From the experimental point of view, this issue is equivalent to attenuating finite-size effects by means of a given quantum protocol<sup>12-14</sup>; analytically, it is an important ingredient for improving numerical methods for many-body systems<sup>15</sup>, such as exact diagonalization<sup>11,16</sup>, Monte Carlo Simulations<sup>17,18</sup> and Renormalization-Groups<sup>19,20</sup>.

In a previous work<sup>21</sup>, we have examined this question by addressing the compatibility between boundary conditions and conserved quantities in the finite one dimensional Hubbard Hamiltonian<sup>22,23</sup>. We analysed some properties of small Hubbard chains under open, periodic and twisted boundary conditions and presented results for the ground state and gap energies, and local densities and magnetizations at half-filling. Special attention was given to the case of twisted boundary conditions<sup>24</sup>, in which the ends of the chain are connected with a hopping amplitude having a torsion phase  $\Theta$ . This situation is physically equivalent to a Hubbard chain coupled to an external vector potential  $A$ . The effect of twisted boundary conditions in integrable models has been widely discussed<sup>24-28</sup>. A vast literature on the low-energy properties covering analytical calculations via Bethe Ansatz of the ground-state energies, correlation functions and order parameters in spin chains, including the Hubbard Hamiltonian<sup>24</sup>. In particular, it has been demonstrated that properties of Hamiltonians obeying  $U(1)$  symmetry do not depend on the boundary condition as the system size is increased, the dependence being exponentially suppressed<sup>24</sup>. Our motivation to revisit the case of finite and relatively small chains has its origins in recent studies of qubit systems. The discussion is linked especially to the experimental realization of protocols engineering few particle systems, which, in practice, are no longer described by integrable models<sup>29,30</sup>. In an attempt to be pedagogical, we demonstrated that there is a special torsion  $\Theta^* = \pi L/2$ , where  $L$  is the system size, in which one can preserve most symmetries of the infinite Hubbard model. We argued that an important consequence of this finding is that under twisted boundary conditions with  $\Theta^*$ , properties converge faster to the limit  $L \rightarrow \infty$ , with excellent results already for relatively small chains of, up to 7 sites.

Here, we complement our analysis of the twisted boundary condition targetting the special property of entanglement. We also provide an instructive description of a flexible numerical procedure based on a binary approach for small spin lattices, used to obtain the results in Ref.<sup>21</sup> and in the present paper. Here, we report numerical calculations for the ground-state energy and the average single-site entanglement, exploring their deviations from the thermodynamical limit ( $L \rightarrow \infty$ ) as a function of the torsion  $\Theta$  and the re-scaled coupling  $U/t$ . Equivalent results could be obtained from the Bethe Ansatz solution of the finite Hubbard Hamiltonian under twisted boundary conditions<sup>31</sup>. Our results indicate that the entanglement under  $\Theta^*$  converges fast, like the ground-state energy. We identify different behaviors in chains with odd and even number of sites and their scaling as  $L$  is increased.

The present paper is organized as follows. In section II we review the connection between symmetries and boundary conditions. In section III, we explain the numerical procedure devised to perform the exact diagonalization of the many-body Hubbard Hamiltonian. Numerical results for the per-site ground-state energy and single-site entanglement of half-filled chains are presented in section IV. Finally, we conclude our analysis on the scaling properties of Hubbard chains under twisted boundary conditions in section V. In appendix B, we also include the case-study of the Hubbard trimer, calculating explicitly the matrix Hamiltonian under twisted boundary condition and presenting analytical results for the single-site entanglement. We show additional results for the deviations from the limit  $L \rightarrow \infty$  in the single-site entanglement as a function of the torsion  $\Theta$  and the coupling  $U/t$  in appendix A.

## II. SYMMETRIES OF THE HUBBARD HAMILTONIAN UNDER TWISTED BOUNDARY CONDITIONS

The Hubbard Hamiltonian is one of the most studied models in condensed matter physics. It has grounded most of our knowledge of a wide class of solid state systems, ranging from conductors to insulators. More recently, it has been successfully used to investigate exotic states of matter occurring in quantum dots<sup>2</sup>, ultracold fermionic atoms and ion traps<sup>1,3</sup>, Bose-Einstein condensates<sup>4</sup>, etc.

Comprising two terms - namely, the hopping and the Coulombian interaction - it translates in a simple way the

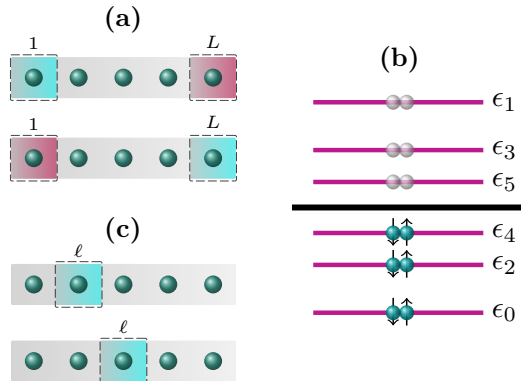


Figure 1. Some of symmetries present in the infinite one-dimensional Hubbard Hamiltonian. **(a)** inversion symmetry: relabelling sites from left to right and vice-versa does not change the transformed Hamiltonian. **(b)** particle-hole symmetry: the energetic cost to add a particle to the first unoccupied level is the same of removing a particle at the last occupied level. **(c)** translation symmetry: the system remains invariant by shifting sites to its neighbors, so that the linear momentum is conserved.

competition between the localization and de-localization trends of quantum particles in a lattice. In one dimension, the fermionic Hubbard Hamiltonian including boundary conditions is written as

$$\begin{aligned} \hat{H} = & -t \sum_{\ell=1}^{L-1} (\hat{c}_{\ell+1}^\dagger \hat{c}_\ell + H.c.) + U \sum_{\ell=1}^L \hat{n}_{\ell\uparrow} \hat{n}_{\ell\downarrow} \\ & - \mu \sum_{\ell=1}^L \hat{n}_\ell + \hat{H}_{BC}, \end{aligned} \quad (1)$$

where the operators  $\hat{c}_\ell$  ( $c_\ell^\dagger$ ) annihilates (creates) an electron at site  $\ell$ ,  $\hat{n}_{\ell,\sigma} = \hat{c}_{\ell,\sigma}^\dagger \hat{c}_{\ell,\sigma}$  counts the occupation of electrons with spin  $\sigma$  at site  $\ell$ ,  $t$  is the hopping amplitude,  $U$  accounts for the Coulomb repulsion penalizing double occupation and  $\mu$  is the chemical potential. The last term connects the ends of the chain  $\ell = 1$  and  $\ell = L$  and defines the boundary condition (BC)

$$\hat{H}_{BC} = -(\tau \hat{c}_1^\dagger \hat{c}_L + \tau^* \hat{c}_L^\dagger \hat{c}_1), \quad (2)$$

so that

$$\tau = \begin{cases} 0 & \text{open (OBC)} \\ t & \text{periodic (PBC)}, \\ te^{i\Theta} & \text{twisted (TBC)} \end{cases} \quad (3)$$

$0 < \Theta < \pi$  being the torsion phase.<sup>32</sup>

Increasing  $L \rightarrow \infty$  and keeping the average electron density constant we recover the thermodynamical limit and the Hamiltonian becomes independent of the boundary condition. This limit is particularly interesting due to the variety of symmetries of the infinite Hubbard chain: besides conserving charge, spin and spin rotation, which are symmetries present also in finite chains under any of the boundary conditions defined in eq. (3), the infinite model also possesses inversion, translation and particle-hole symmetry; the latter having a crucial role. An illustration of the last three is shown in figure 1 and a complete discussion can be found in ref.<sup>21</sup>. Here, we recapitulate, in more detail, the derivation of the condition that the twist phase  $\Theta$  must fulfill to preserve particle-hole and translation symmetries in a finite Hubbard chain under twisted boundary condition.

In the presence of particle-hole symmetry, the cost for adding or removing a particle from the Fermi level is the same. The Hamiltonian must be invariant under the transformation

$$\hat{c}_\ell \rightarrow (-1)^\ell \hat{a}_\ell^\dagger. \quad (4)$$

Carrying out the transformation for the Hamiltonian under open boundary condition  $\hat{H}_{OBC}$ , we find

$$\begin{aligned}\hat{H}_{OBC} &= -t \sum_{\ell=1}^{L-1} (-1)^{2\ell+1} (\hat{a}_{\ell+1} \hat{a}_{\ell}^{\dagger} + \hat{a}_{\ell} \hat{a}_{\ell+1}^{\dagger}) + U \sum_{\ell=1}^L (-1)^{4\ell} \hat{a}_{\ell\uparrow} \hat{a}_{\ell\uparrow}^{\dagger} \hat{a}_{\ell\downarrow} \hat{a}_{\ell\downarrow}^{\dagger} - \mu \sum_{\ell=1}^L (-1)^{2\ell} (\hat{a}_{\ell\uparrow} \hat{a}_{\ell\uparrow}^{\dagger} + \hat{a}_{\ell\downarrow} \hat{a}_{\ell\downarrow}^{\dagger}) \\ &= -t \sum_{\ell=1}^{L-1} (\hat{a}_{\ell}^{\dagger} \hat{a}_{\ell+1} + \hat{a}_{\ell+1}^{\dagger} \hat{a}_{\ell}) + U \sum_{\ell=1}^L \hat{a}_{\ell\uparrow}^{\dagger} \hat{a}_{\ell\uparrow} \hat{a}_{\ell\downarrow}^{\dagger} \hat{a}_{\ell\downarrow} - \mu \sum_{\ell=1}^L (\hat{a}_{\ell\uparrow}^{\dagger} \hat{a}_{\ell\uparrow} + \hat{a}_{\ell\downarrow}^{\dagger} \hat{a}_{\ell\downarrow}),\end{aligned}\quad (5)$$

so that the open chain remains invariant.

Carrying out the transformation for  $\hat{H}_{BC}$ , we obtain

$$\begin{aligned}\hat{H}_{BC} &= -(\tau(-1)^1 \hat{a}_1 (-1)^L \hat{a}_L^{\dagger} + \tau^* (-1)^L \hat{a}_L (-1)^1 \hat{a}_1^{\dagger}) \\ &= (-1)^{L+1} \tau \hat{a}_L^{\dagger} \hat{a}_1 + (-1)^{L+1} \tau^* \hat{a}_1^{\dagger} \hat{a}_L.\end{aligned}\quad (6)$$

To respect particle-hole symmetry, the hopping amplitude in the boundary must fulfill the condition

$$(-1)^{L+1} \tau^* = -\tau. \quad (7)$$

As shown in Ref.<sup>21</sup>, condition (7) is fulfilled if the torsion is adjusted as follows

$$\Theta^* = \frac{\pi L}{2}. \quad (8)$$

For  $0 \leq \Theta \leq \pi$ , the previous relation split the cases of even and odd  $L$ 's

$$\begin{aligned}\Theta_{\text{odd}}^* &= \frac{\pi}{2} \\ \Theta_{\text{even}}^* &= \begin{cases} 0, & L/2 \text{ even} \\ \pi, & L/2 \text{ odd} \end{cases}.\end{aligned}\quad (9)$$

Now, we can carry out a similar sequence of steps to find the conditions for the phase  $\Theta$  so that the system conserves momentum. Starting from the transformation

$$\hat{c}_{\ell} \rightarrow e^{i\ell\theta} \hat{a}_{\ell}, \quad (10)$$

and inserting it into  $\hat{H}$  only change the first and last terms of eq. (1), giving

$$-t \sum_{\ell=1}^{L-1} (\hat{c}_{\ell+1}^{\dagger} \hat{c}_{\ell} + H.c.) = - \sum_{\ell=1}^{L-1} (e^{-i\theta} \hat{a}_{\ell+1}^{\dagger} \hat{a}_{\ell} + e^{+i\theta} \hat{a}_{\ell+1}^{\dagger} \hat{a}_{\ell}), \quad (11)$$

and

$$\hat{H}_{BC} = -t(e^{i(L-1)\theta+\Theta} \hat{a}_1^{\dagger} \hat{a}_L + e^{-i(L-1)\theta-\Theta} \hat{a}_L^{\dagger} \hat{a}_1). \quad (12)$$

The invariance of the Hamiltonian under (10) requires

$$\theta = \frac{\Theta}{L}, \quad (13)$$

which is equivalent of implementing a local twist through the hopping amplitudes

$$t \rightarrow te^{i\theta}, \quad (14)$$

so that the torsion  $\Theta$  is distributed along the chain.

These valuable findings bring the interesting question of how properties in the thermodynamical limit compare with those in finite chains when the boundary conditions fulfill conservation laws. Here, we are going to examine the dependencies of energies and correlations with the torsion  $\Theta$ , discussing their convergence to their values for the infinite Hubbard model calculated exactly with the Bethe Ansatz.

We now consider the distances  $\Delta\epsilon_p = |\epsilon_p(L, n, U, \Theta) - \epsilon_p^{BA}(n, U)|$  between the Bethe Ansatz density energies  $\epsilon_p^{BA}(U, n)$  for the infinite Hubbard model with filling  $n$  and

$$\epsilon_p(L, n, U, \Theta) = \frac{1}{tL} \langle \Psi_p | \hat{H}(L, n, U, \Theta) | \Psi_p \rangle, \quad (15)$$

is the per-site energy, where  $|\Psi_p\rangle$  is the exact  $p$ -th state of  $\hat{H}$  ( $p = 0$  corresponds to the ground-state,  $p = 1$  corresponds to the first excited state and so on) calculated for a chain with  $L$  sites,  $Q = nL$  particles, coupling  $U$  and torsion  $\Theta$ .

In particular, the ground-state density energy  $\epsilon_0(L, n = 1, U, \Theta)$  at half-filling ( $n = 1$  or  $Q = L$ ) will be compared with the Bethe Ansatz ground-state energy for the infinite half-filled Hubbard model, calculated from

$$\epsilon_0^{BA}(n = 1, U) = -4 \int_0^\infty dx \frac{J_0(x)J_1(x)}{x[1 + e^{Ux/2}]}. \quad (16)$$

The single-site entanglement can be quantified by means of the Von Neumann entropy

$$S(\rho_\ell) = - \sum_p \lambda_p \log(\lambda_p), \quad (17)$$

where  $0 \leq \lambda_p \leq 1$  are the eigenvalues of the reduced density matrix  $\rho_\ell = \text{Tr}_{k \neq \ell} [\rho]$ , defined for pure states  $\rho = |\Psi\rangle \langle \Psi|$  and obtained by tracing all the degrees of freedom of the system excluding the degrees of freedom of site  $\ell$ .

For fermions, the reduced density matrix is a  $4 \times 4$  diagonal matrix whose eigenvalues correspond to the probabilities to find the  $\ell$ -th site empty ( $\lambda_0$ ), single ( $\lambda_\uparrow$  and  $\lambda_\downarrow$ ) or double occupied ( $\lambda_\uparrow\downarrow$ ). Explicitly, it reads

$$\rho_\ell = \begin{pmatrix} \lambda_0 & 0 & 0 & 0 \\ 0 & \lambda_\downarrow & 0 & 0 \\ 0 & 0 & \lambda_\uparrow & 0 \\ 0 & 0 & 0 & \lambda_{\uparrow\downarrow} \end{pmatrix}. \quad (18)$$

In our comparison of the average single-site entanglement entropy  $\langle S_j \rangle(L, n, U, \Theta^*)$  with the Bethe Ansatz results for the infinite Hubbard model, we will rely on the analytical expression derived in Refs.<sup>33-35</sup>. It reads

$$\langle S_j \rangle(n, U) = -2 \left( \frac{n}{2} - \frac{\partial \epsilon}{\partial U} \right) \log_2 \left[ \frac{n}{2} - \frac{\partial \epsilon}{\partial U} \right] - \left( 1 - n + \frac{\partial \epsilon}{\partial U} \right) \log_2 \left[ 1 - n + \frac{\partial \epsilon}{\partial U} \right] - \frac{\partial \epsilon}{\partial U} \log_2 \left[ \frac{\partial \epsilon}{\partial U} \right], \quad (19)$$

where  $\epsilon = \epsilon_0^{BA}(n, U)$  is the per-site ground-state energy, which will be computed from the Bethe Ansatz at half-filling  $n = 1$  as indicated in eq. (16).

The numerical procedure we used to obtain these properties in the case of finite lattices with given torsion  $\Theta$  is described in the next section.

### III. EXACT DIAGONALIZATION PROCEDURE

The complete Hilbert space of a fermionic Hubbard chain with  $L$  sites comprises  $4^L$  states, as each site can be empty, singly occupied with  $\sigma = \uparrow, \downarrow$  or doubly occupied. In practice, carrying out the diagonalization of the full matrix Hamiltonian is limited to few sites, of the order of ten. The conservation of charge and spin allows us to bring the Hamiltonian (1) into a block diagonal form, so that each block  $H(Q, S)$  is associated with a smaller Hilbert space  $(Q, S)$  formed by states with definite charge  $Q$  and spin  $S$ . For chain with  $L \leq 9$  sites, the number of states in the largest subspace  $(Q, S)$  (8820 states) can still be handled exactly without high computational efforts. In practice, larger matrices  $L > 10$  would require the use of special techniques for storing and diagonalizing the matrix Hamiltonian  $H(Q, S)$ , i.e., a large space in memory RAM and a longer time to perform the diagonalization, whose complexity order scales with  $\mathcal{O}(n^3)$ , where  $n$  is the dimension of the problem.

In the present work, we implemented an exact diagonalization procedure in which the fermionic states are represented in a binary notation<sup>36,37</sup>. The use of hashing tables, like the binary notation, to represent quantum states of spin models is a convenient choice in exact diagonalization procedures, including the Lanczos algorithm<sup>36,38</sup>. The latter allows to obtain with high accuracy the low-energy spectrum of chains with up to  $L = 24$  sites<sup>37</sup> for open boundary conditions and  $L = 12$  for twisted boundary conditions<sup>31,38</sup>, the latter being halved because the twist phase introduces complex numbers in the Hamiltonian matrix therefore requiring the double of space and more computation time compared to real matrices.

Here, we will describe a simple formulation of a binary hashing to represent quantum states of one-dimensional fermionic systems, from which one is able to obtain exactly the full spectrum of the Hamiltonian  $H(Q, S)$  using a standard diagonalization routine. Differently from other methods, such as the Lanczos diagonalization, the procedure yields all the  $4^L$  eigenstates and eigenvalues of the full many-body Hamiltonian without any approximation or truncation. The procedure comprises three steps: the binary representation of basis elements in the subspace  $(Q, S_z = S)$ , the rotation of the basis in  $(Q, S_z)$  to the subspace  $(Q, S)$ , and the projection of the Hamiltonian operator into the basis elements forming the subspace  $(Q, S)$ .

The first step of the exact calculation involves the definition of the hashing code to represent fermionic states in the binary form. Given a lattice of  $L$  sites, each one of the  $n_B = 2^{2L}$  possible spin configurations  $|\vec{\sigma}\rangle = |\sigma_1\rangle \otimes |\sigma_2\rangle \otimes \dots \otimes |\sigma_L\rangle$  is associated with a sequence of  $2L$  bits, the even indexes referring to occupations of  $\uparrow$  and the odd indexes referring to occupations of  $\downarrow$ , i.e.

$$\begin{aligned} |b\rangle &= |b_{1\uparrow} b_{1\downarrow} b_{2\uparrow} b_{2\downarrow}, \dots, b_{L\uparrow} b_{L\downarrow}\rangle \\ &= |\sigma_1\rangle \otimes |\sigma_2\rangle \otimes \dots \otimes |\sigma_L\rangle, \end{aligned} \quad (20)$$

where  $b_{\ell\sigma}$  ( $\ell = 1, \dots, L$ ) can be either 0 or 1.  $b_{\ell\uparrow} = 1$  means that there is an electron  $\uparrow$  in the  $\ell$ -th site (it is equivalent to the creation operator  $c_{\ell\uparrow}^\dagger$ ), whereas  $b_{\ell\uparrow} = 0$  indicates that site  $\ell$  does not have an electron  $\uparrow$ . Likewise,  $b_{\ell\downarrow} = 1$  is equivalent to  $c_{\ell\downarrow}^\dagger$  and  $b_{\ell\downarrow} = 0$  is equivalent to  $c_{\ell\downarrow}$ . Some examples are illustrated in figure 2.

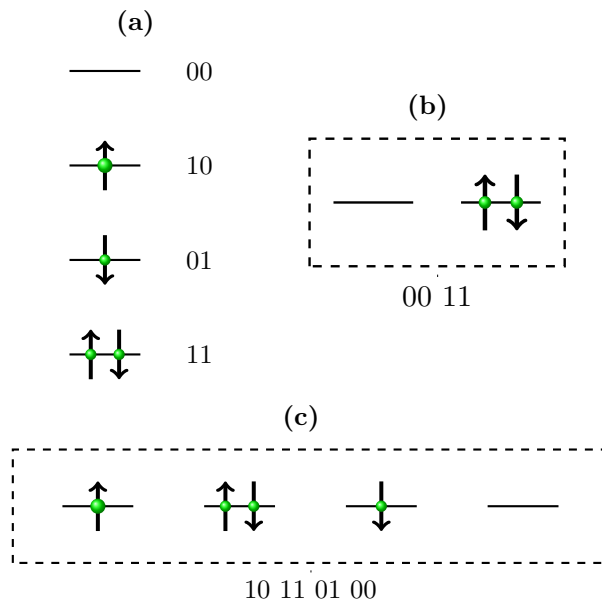


Figure 2. Binary representation of fermionic configurations  $|b\rangle$ . Examples of configurations for (a) single-site with  $i_b = 0, 2, 1, 3$  from top to bottom; (b) dimer  $L = 2$  with  $i_b = 3$ ; and (c) tetramer  $L = 4$  and  $i_b = 180$ .

We can ascribe an integer label  $i_b = 0, \dots, n_B - 1$  to each binary configuration  $|b\rangle$ , so that

$$i_b = \sum_{\ell=1}^L (b_{\ell\uparrow} 2^{2L-\ell} + b_{\ell\downarrow} 2^{2L-\ell-1}). \quad (21)$$

The label  $i_b$  provides all information of the spin state  $\sigma_\ell$  of each site  $\ell$ . For instance,

$$b_{\ell\uparrow} = \text{mod}_2 \left[ \frac{i_b}{2^{2L-2\ell+1}} \right], \quad (22)$$

and

$$b_{\ell\downarrow} = \text{mod}_2 \left[ \frac{i_b}{2^{2L-2\ell}} \right]. \quad (23)$$

The action of any operator  $\hat{O}$  on any state of the complete Hilbert space written in the binary form of eq. (21) only requires the definition of such operator in terms of bit operations. For instance, the action of the creation and annihilation operators  $\hat{c}_{\ell\uparrow}^\dagger$  and  $\hat{c}_{\ell\uparrow}$  ( $\ell = 1, \dots, L$ ) in a state  $|i_b\rangle$  labeled by  $i_b$  can be defined as

$$\begin{aligned}\hat{c}_{\ell\uparrow}^\dagger |i_b\rangle &\equiv \frac{1}{2}(1 + (-1)^{b_{\ell\uparrow}}) |i_b + 2^{2(L-\ell)+1}\rangle \\ \hat{c}_{\ell\uparrow} |i_b\rangle &\equiv \frac{1}{2}(1 + (-1)^{1+b_{\ell\uparrow}}) |i_b + 2^{2(L-\ell)+1}\rangle.\end{aligned}\quad (24)$$

Similar relations can be defined for the  $\downarrow$  spins, replacing  $2\ell \rightarrow 2\ell - 1$  and adding an extra factor  $(-1)^{b_{\ell\uparrow}}$  accounting for the fermionic signals.

As an example, consider the state  $|i_b = 9\rangle = |1001\rangle$  and the action of the operators  $\hat{c}_{1\downarrow}^\dagger$  and  $\hat{c}_{2\uparrow}$ . It follows that

$$\begin{aligned}\hat{c}_{1\downarrow}^\dagger |i_b = 9\rangle &= \frac{1}{2}(1 + (-1)^0) |9 + 2^{2(2-1)}\rangle = |\tilde{i}_b = 13\rangle \\ \hat{c}_{2\uparrow} |i_b = 9\rangle &= \frac{1}{2}(1 + (-1)^1) |9 + 2^{2(2-2)+1}\rangle = 0 |\tilde{i}_b = 11\rangle.\end{aligned}\quad (25)$$

Notice that while the operation  $\hat{c}_{1\downarrow}^\dagger |i_b = 9\rangle$  yields a new binary index  $\tilde{i}_b = 13$  which reconstructs the binary state  $|1101\rangle$ , the action of  $\hat{c}_{2\uparrow}$  on  $|i_b = 9\rangle$  does not produce a new binary configuration, as the spin  $\uparrow$  of the second site is empty.

Once defined the operators composing the Hamiltonian in terms of binary relations, we are able to proceed and construct the corresponding matrix  $H$  in the subspaces of states with definite charge and spin. Within the binary approach, the subspaces  $(Q, S)$  can be obtained in two steps. First, we need to identify the  $n_B$  configurations constrained by

$$\sum_{\ell=1}^L b_{\uparrow\ell} + b_{\downarrow\ell} - L = Q, \quad (26)$$

$$\sum_{\ell=1}^L b_{\uparrow\ell} - b_{\downarrow\ell} = S_z, \quad (27)$$

which form the Hilbert space  $(Q, S_z)$  of eigenstates of the operators  $\hat{Q}$  and  $\hat{S}_z$ , defined as

$$\hat{Q} = \sum_{\ell=1}^L \sum_{\sigma=\uparrow,\downarrow} (\hat{c}_{\ell\sigma}^\dagger \hat{c}_{\ell\sigma} - \frac{1}{2}), \quad (28)$$

and

$$\hat{S}_z = \frac{1}{2} \sum_{\ell=1}^L \sum_{\mu,\nu=\uparrow,\downarrow} \hat{c}_{\ell\mu}^\dagger \sigma_{\mu,\nu}^z \hat{c}_{\ell\nu}, \quad (29)$$

where  $\sigma^z$  is the  $z$  component of the Pauli matrices.

The subspace  $(Q, S_z)$  comprises  $n_B$  binary configurations forming the basis  $\{|q, s_z, b\rangle\}$  ( $b = 0, 1, \dots, n_B - 1$ ), where

$$\begin{aligned}\hat{Q} |q, s_z, b\rangle &= Q |q, s_z, b\rangle \\ \hat{S}_z |q, s_z, b\rangle &= S_z |q, s_z, b\rangle\end{aligned}\quad (30)$$

for all  $b = 0, \dots, n_B - 1$ .

The conservation of the total spin  $S$  yields a new projection of the Hamiltonian into the subspace  $(Q, S)$  comprising  $n_P < n_B$  eigenstates  $\{|q, s, s_z = s, p\rangle\}$  ( $p = 0, \dots, n_P - 1$ ) of the operator

$$\hat{\tilde{S}} = \frac{1}{2} \sum_{\ell=1}^L \sum_{\mu,\nu=\uparrow,\downarrow} \hat{c}_{\ell\mu}^\dagger \vec{\sigma}_{\mu,\nu} \hat{c}_{\ell\nu}, \quad (31)$$

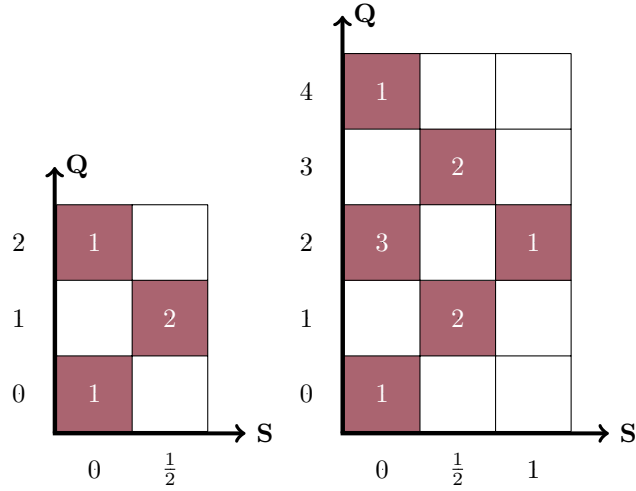


Figure 3. Board of active sectors  $(Q, S)$  in the iterations  $\ell = 1$  and  $\ell = 2$  and the number  $p$  of states  $|q, s, s = s_z, p, \ell\rangle$  with definite charge and spin inside them. Colored squares indicate the active sectors of the current chain. White numbers mean the number of states in each sector.

where  $\vec{\sigma} = \sigma_x \hat{x} + \sigma_y \hat{y} + \sigma_z \hat{z}$ .

All  $n_P$  basis elements in the subspace  $(Q, S)$  satisfy

$$\hat{S}^2 |q, s, s_z = s, p\rangle = s(s+1) |q, s, s_z = s, p\rangle. \quad (32)$$

Having the  $n_B$  eigenstates  $\{|q, s_z, b\rangle\}$  and definitions for the operators in the binary notation, the projection of the Hamiltonian  $\hat{H}$  into a basis defining the subspace  $(Q, S)$  requires the transformation  $\mathcal{T}_{p,b}$  rotating the basis  $\{|q, s_z, b\rangle\}$  in  $(Q, S_z)$  into the new basis  $\{|q, s, s_z = s, p\rangle\}$  in  $(Q, S)$ . This can be done using two approaches. We can define the operator  $\hat{S}^2$  in the binary form, project it into the basis  $\{|q, s_z, b\rangle\}$  and from the diagonalization of the matrix  $S^2$  identify the eigenstates with  $s$  and  $s_z = s$ . Alternatively and, more efficiently, we implement an iterative procedure in which the Hilbert spaces  $(Q, S)$  are constructed by growing the chain from  $\ell = 1$  to  $\ell = L$  and finding the eigenstates  $|q_\ell, s_\ell, s_{z\ell}, p_\ell\rangle_\ell$  with help of the rules of addition of angular momenta.

We start with all eigenstates  $|q_{\ell=1}, s_{\ell=1}, s_z = s, p_{\ell=1}\rangle$  for a single site in the end of the chain, which are

$$\begin{aligned} |q = 0, s = 0, s_z = 0, p = 0\rangle_{\ell=1} &= |0\rangle \\ |q = 1, s = +\frac{1}{2}, s_z = +\frac{1}{2}, p = 0\rangle_{\ell=1} &= \hat{c}_{L\uparrow}^\dagger |0\rangle \\ |q = +2, s = 0, s_z = 0, p = 0\rangle_{\ell=1} &= \hat{c}_{L\uparrow}^\dagger \hat{c}_{L\downarrow}^\dagger |0\rangle. \end{aligned} \quad (33)$$

These states are stored in a board of active sectors, as illustrated in figure 3. The next step is adding the site  $L - 1$  with Clebsch-Gordan coefficients to obtain the eigenstates of  $|q_{\ell=2}, s_{\ell=2}, s_z = s, p_{\ell=2}\rangle$ , which are stored in a new set of active sectors in the board. For this, we use the following relations

$$|q, s, s_z, p'\rangle_{\ell+1} = |q + 1, s, s_z, p'\rangle_\ell \quad p' = 0, \dots, n_P(q + 1, s)_\ell, \quad (34)$$

$$\begin{aligned} |q, s, s_z, p'' + \max p'\rangle_{\ell+1} &= c_{L-\ell\uparrow}^\dagger |q, s - \frac{1}{2}, s_z - \frac{1}{2}, p''\rangle_\ell \\ p'' &= 0, \dots, n_P(q, s - \frac{1}{2})_\ell, \end{aligned} \quad (35)$$



$$\begin{aligned}
|q, s, s_z, p''' + \max p' + \max p''\rangle_{\ell+1} &= \frac{-1}{\sqrt{2s+1}} c_{L-\ell\uparrow}^\dagger |q, s + \frac{1}{2}, s_z - \frac{1}{2}, p'''\rangle_\ell \\
&+ \sqrt{\frac{2s}{2s+1}} c_{L-\ell\downarrow}^\dagger |q, s + \frac{1}{2}, s_z + \frac{1}{2}, p'''\rangle_\ell \\
p''' &= 0, \dots, n_P(q, s + \frac{1}{2})_\ell,
\end{aligned} \tag{36}$$

$$\begin{aligned}
|q, s, s_z, p'''' + \max p' + \max p'' + \max p'''\rangle_{\ell+1} &= c_{L-\ell\uparrow}^\dagger c_{L-\ell\downarrow}^\dagger |q-1, s, s_z, p''''\rangle_\ell \\
p'''' &= 0, \dots, n_P(q-1, s)_\ell.
\end{aligned} \tag{37}$$

Notice that, due to the degeneracy of the  $z$  components of momentum, fixing  $s_z = s$  is convenient to save memory, so that we do not need to store all the  $s_z$  components of  $s$  (states  $|q, s, s_z \neq +s, p\rangle$ ) because they can be simply recovered from  $|q, s, s_z = +s, p\rangle$ . For example, the configurations  $|q, s, s_z = s-1, p\rangle_\ell$  needed to construct states  $|q, s \pm 1/2, s_z \pm 1/2, p\rangle_{\ell+1}$  from the ones obtained in the last iteration -  $|q, s, s_z = s, p\rangle_\ell$  in eqs. (35) and (36)- can be implemented easily by flipping all the spins  $\uparrow$  of the previously stored  $|q, s, s_z = s, p\rangle_\ell$ .

The growing procedure is repeated until  $\ell = L$ , yielding all the rotation matrices  $\mathcal{T}_{p,b}(Q, S)$  for each subspace  $(Q, S)$  and their binary states  $|b\rangle$ . Using the bit rules for the action of the operators defining the Hamiltonian  $\hat{H}$ , the matrix elements of  $H(Q, S_z)$  are calculated as

$$H_{b,b'} = \langle i_b | \hat{H} | i_{b'} \rangle, \tag{38}$$

where  $i_b$  and  $i_{b'}$  label the binary configurations  $|b\rangle$  and  $|b'\rangle$  of  $(Q, S)$ .

The rotation  $\mathcal{T}_{p,b}(Q, S)$  is then applied, resulting in a matrix  $n_P \times n_P$ , i.e.,

$$H(Q, S) = \mathcal{T}_{p,b}(Q, S) H(Q, S_z) \mathcal{T}_{p,b}^{-1}(Q, S), \tag{39}$$

which can be diagonalized.

In the table below, we present some examples of numbers  $n_P$  and  $n_B$  as a function of  $L$ .

$L$	$n_P$	$n_B$
2	3	4
3	6	9
4	20	36
5	75	100
6	175	400
7	784	1225
8	1764	4900
9	8820	15876
10	19404	63504

Table I. Highest number  $n_P$  of states in local Hilbert spaces  $(Q, S)$  and number  $n_B$  of binary configurations needed to generate them as a function of  $L$ . For even  $L$ , the most dense Hilbert space is  $(Q = L, S = 0)$ , whereas for  $L$  odd it is  $(Q = L, S = \frac{1}{2})$ .

Under twisted boundary conditions, once the matrix elements of  $H$  are complex, effectively, the memory needed to store the full Hamiltonian is  $n_P^2$  double precision floating points, which is twice the capacity needed for open and periodic boundary conditions.

The procedure introduced above was used in our numerical calculations of the ground-state energy and single site entanglement presented in section II. Besides the ground-state properties, our code provides the full excitation spectrum of  $H(Q, S)$  for any coupling  $U$  and torsion  $\Theta$ . It also offers a flexible framework with support for non-homogeneous model parameters, non-local interactions and time-dependent calculations. For the purposes of the present paper, we will focus our analysis on the case of half-filled chains  $Q = L$  and  $S = 0$  ( $L$  even) or  $S = 1/2$  ( $L$  odd). Our results are presented below.

#### IV. RESULTS

In the infinite chain, ground-state properties at half-filling capture the rich physics regarding the phases of the Hubbard model. For  $U = 0$ , the Hamiltonian  $\hat{H}(L \rightarrow \infty)$  reduces to a free electron gas, as the electrons can move freely along the chain through the kinetic hopping. In the presence of non-zero coupling, even infinitesimal, the system enters in an insulating phase, with gap energy  $\Delta$  increasing with  $U/t$ . In the limit  $U \rightarrow \infty$ , the prohibitive cost of double occupation leads the system to become a Néel antiferromagnetic insulator. The change in the behavior of properties during the transition from the non-interacting ( $U/t \rightarrow 0$ ) to extreme Mott insulating ( $U/t \gg 1$ ) phase is noticeable, as illustrated in figure 4. The per-site ground-state energy starts from its minimum value  $\epsilon_0^{BA}(n=1, U \rightarrow 0) \approx -4/\pi$  and increases up to zero, when electrons freeze in a state whose components only assume single occupation. See figure 4(a).

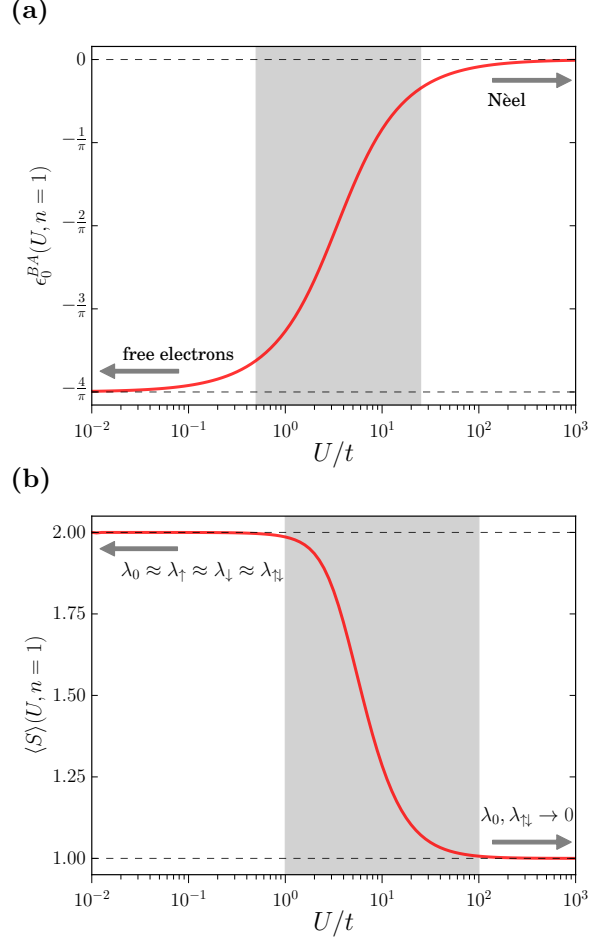


Figure 4. Ground-state energy (a) and single-site entanglement entropy (b) for the infinite 1-D Hubbard model computed from the Bethe Ansatz solution at half-filling - eqs. (16) and (19). The behavior of both quantities illustrates two solid state phases of the Hubbard model: a tight-binding model for a free electron gas when the coupling is absent ( $U = 0$ ) and a Néel antiferromagnetic insulator in the limit  $U \rightarrow \infty$ . In the shaded in region (gray), the Coulomb repulsion is not negligible nor high enough, so that competing correlations exist in the ground-state wave function.

The transition between these two extremes is particularly interesting when we analyse internal correlations by means of the average single-site entanglement, shown in figure 4(b). When  $U = 0$ , the ground-state wave-function  $|\Psi_0\rangle$  decomposes in a Slater determinant of single-site orbitals with equal contribution. Inspection of eq. (18) provides a limiting value for  $\langle S_j \rangle(U \rightarrow 0) \rightarrow 2$ , when all the eigenvalues of the reduced density matrix are degenerate, i.e.,  $\lambda_0 \approx \lambda_\uparrow \approx \lambda_\downarrow \approx \lambda_{\uparrow\downarrow} \approx 1/4$ . In this limit, all individual sites become uniformly coupled to the rest of the chain, so that the entropy reaches its maximum. In the presence of coupling, the competition between the scales  $t$  and  $U$  results in a complex ground-state, whose components are formed by spin configurations with non-trivial occupation probabilities

$\lambda_0 \neq \lambda_\uparrow \neq \lambda_\downarrow \neq \lambda_\updownarrow$ . The sensitivity of  $|\Psi_0\rangle$  to the Coulomb repulsion manifests in the measure of the average single-site entanglement, as  $\langle S_j \rangle$  decreases almost ballistic within the range  $1 \leq U/t \leq 10^2$ . Outside this region and, in particular, for very large coupling, empty and double occupations vanish  $\lambda_0, \lambda_\updownarrow \rightarrow 0$ . The entropy reaches half of its maximum, as the components of  $|\Psi_0\rangle$  formed by single occupied sites contributes equally  $\lambda_\uparrow \approx \lambda_\downarrow \rightarrow 1/2$ . We note that this corresponds to the maximum entropy of the halved Hilbert space.

We can now examine how far from the thermodynamical limit are these quantities in the case of finite chains under twisted boundary conditions. We vary the torsion of  $\pi$  around the special phases  $\Theta_{\text{odd}}^*$  or  $\Theta_{\text{even}}^*$  under which the system possesses particle-hole and translation symmetries. In order to extend the previous analysis about the correspondence between the the phases of the Hubbard Hamiltonian and its coupling regimes, we keep the Coulomb repulsion within the range  $10^{-2} < U/t < 10^3$ .

Initially, we consider the deviations in the per-site ground-state energy from the thermodynamical limit of the one-dimensional Hubbard Hamiltonian at half-filling, analysing the dependences on the coupling  $U/t$  and the torsion  $\Theta$ . Here, we argue that working with the absolute difference instead of the percentual deviation is more convenient in the comparison of the ground-state energy because it avoid numerical divergences in the limits ( $U \gg 10t$ ) where  $\epsilon_0$  vanishes. Explicitly,  $\Delta\epsilon_0$  is calculated as follows

$$\Delta\epsilon_0(L, n = 1, U, \Theta) = |\epsilon_0(L, n = 1, U, \Theta) - \epsilon_0^{BA}(n = 1, U)|. \quad (40)$$

Figures 5 and 6 show  $\Delta\epsilon_0$  as a function of  $U/t$  and  $\Theta$  for odd and even number of lattice sites, respectively. The dependence of  $\Delta\epsilon_0$  on  $\Theta$  is only appreciable in low and intermediate coupling regimes, where we identify a periodic behavior which differ among chains with odd and even number of sites. The difference between  $L$  odd and  $L$  even can be understood easily by inspecting the non-interacting limit ( $U = 0$ ), for which the deviations are maximized. For  $L$  even, the Hamiltonian remains invariant under inversion. Under the special torsion  $\Theta^*$  for  $U = 0$  and even  $L$ , several of the single-particle levels with nonzero momentum are degenerate. For  $L$  odd, the Hamiltonian breaks inversion symmetry and the single-particle levels are not degenerate. As the degeneracy of levels for  $L$  even leads to a relatively poor representation of the thermodynamical limit, it follows that  $\Theta^*$  preserving particle-hole symmetry maximizes the deviation from the Bethe Ansatz solution for  $L \rightarrow \infty$ . By contrast, in chains with odd number of sites (for which the single-particle levels are non-degenerate), the special condition minimizes the deviation. This analysis can be extended for the interacting Hubbard Hamiltonian. Moreover, if we consider  $\Theta$  varying from 0 to  $L\pi$ , we will observe  $L$  minima for both even and odd chains, their position being  $(2n + 1)\pi/2$   $n = 1, \dots, L$ . The maxima, occur in the mid points of the minima and differ between even and odd chains. Inspecting panels **(a)**-**(c)** of Fig. 5, we observe two maxima in the deviations at points  $\Theta^* \pm \pi/2$  for  $L = 3, 5, 7$ . Panels **(a)**-**(c)** of Fig. 6 reveal a different structure: the highest deviation from the Bethe Ansatz occur exactly at the special torsion  $\Theta^*$ , and two local maxima with a smaller amplitude is found at the points  $\Theta^* \pm \pi$ . This corresponds to a different periodicity around the special torsion  $\Theta^*$ : for  $L$  odd, the behavior repeats around  $\Theta^* \pm \pi/2$ , while for even  $L$ , the periodicity of properties occur around  $\Theta^* \pm \pi$ .

Comparison of panels **(a)**-**(c)** in figures 5 and 6 within the coupling region limited by  $U/t < 10$ , indicates the lowest deviations in the energy for  $L = 3, 5$  and 7 occurring exactly at  $\Theta_{\text{odd}}^*$ , whereas for  $L = 4, 6$  and 8,  $\Delta\epsilon_0$  reaches its maximum value for  $\Theta_{\text{even}}^*$ . Clearly, increasing  $L$  ensures convergence to the thermodynamical limit. Following panels **(a)** to **(c)** in figure 5, we observe the highest deviations decrease from  $\Delta\epsilon_0 \approx 0.3$  for  $L = 3$  to one order below  $\Delta\epsilon_0 \approx 0.05$  for  $L = 7$ . In the case of  $L$  even, shown in 6**(a)**-**(c)**, we note that the upper limit of  $\Delta\epsilon_0$  is of the same order of those found in  $L - 1$ , with the correspondence  $L = 3$  and  $L = 4$ ,  $L = 5$  and  $L = 6$ , and  $L = 7$  and  $L = 8$ . When the system approaches the Nèel state, the lowest absolute differences in energy are  $\Delta\epsilon_0 \approx 10^{-4}$  for  $L$  up to 7 and  $\leq 5 \times 10^{-5}$  for  $L = 8$ .

The case in which the special torsion  $\Theta^*$  ensures particle-hole symmetry is presented in panel **(d)** of figures 5 and 6. Under  $\Theta^*$ , deviations from the thermodynamical limit are nearly constant for  $U/t < 1$ , and depict a rapid decreasing up to  $U/t < 100$ , when the system becomes antiferromagnetic. The shaded region distinguishes the limits of couplings for which the system is away from either the single-particle and the Nèel states. For both odd and even chains,  $\Delta\epsilon_0(U, \Theta^*)$  depicts a local minimum followed by a local maximum. We observe the inflection points occurring at different positions  $U^*(L)$  in the axis  $U/t$ , indicating the scaling of  $\epsilon_0(L, \Theta^*)$ , as for example,  $U^*(L = 7) < U^*(L = 5) < U^*(L = 3)$ , and similarly, with  $L$  even.

The analysis of the transition from the non-interacting ( $U = 0$ ) to the Nèel insulating phase ( $U/t \rightarrow \infty$ ) - shaded region in panel **(d)** in figures 5 and 6 - can be better understood in terms of the average single-site entanglement  $\langle S_j \rangle$ , which has been recently proposed as a witness of quantum phase transition<sup>9,39-42</sup>. An important observation concerns the homogeneity of single-site entanglement along the chain, which is highly sensible to closed or open boundary conditions. As discussed in Ref.<sup>21</sup>, local densities and magnetizations vary from site to site under open boundary conditions. Under twisted boundary conditions, a special case of closed boundary conditions, the densities are uniform and independent of  $U/t$  and so does  $S_j = \langle S_j \rangle$ . Nevertheless, the strength of  $U/t$  modifies the inner structure of the ground-state wave-function and this dependence must be reflected in correlation measurements, such

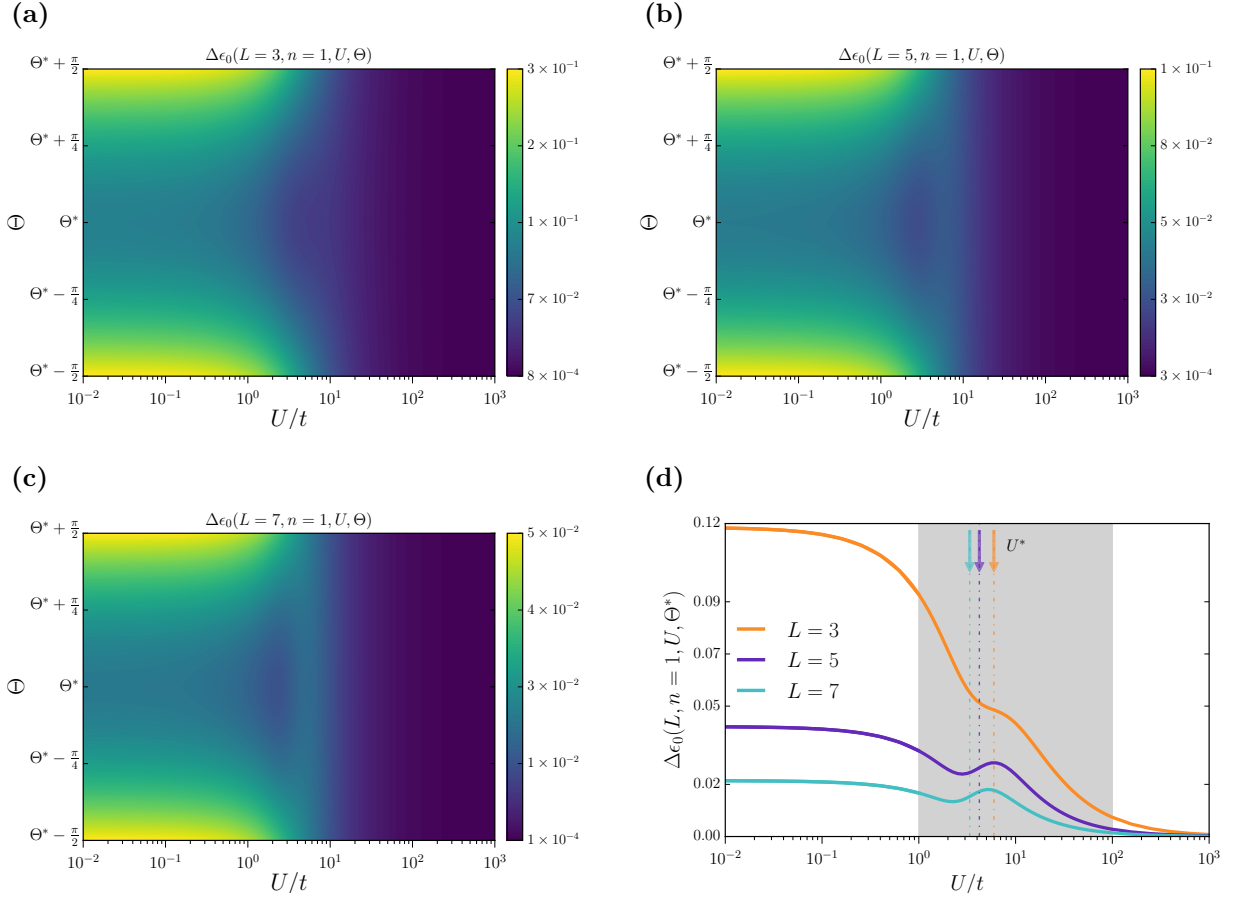


Figure 5. Deviations in the per-site ground-state density energies  $\epsilon_0(L, n = 1, U, \Theta)$  of finite Hubbard chains from the thermodynamical limit  $\epsilon_0^{BA}(n = 1, U)$  calculated from the Bethe Ansatz. Panels (a), (b) and (c) show  $\Delta\epsilon_0(L, n = 1, U, \Theta)$  as a function of the torsion  $\Theta$  and the coupling  $U/t$  for lattices with  $L = 3, 5$  and  $7$ , respectively. Panel (d) displays  $\Delta\epsilon_0(L, n = 1, U, \Theta^*)$  under the special torsion  $\Theta_{\text{odd}}^* = \pi/2$  and highlight the couplings  $U^*/t$  where the deviations present an inflection point. The highest deviations from the thermodynamical limit  $L \rightarrow \infty$  are found in the non-interacting and intermediate coupling regimes ( $U/t < 10$ ).

as the entanglement. In that sense, our proposal to examine the effects of the twisted boundary condition in the average single-site entanglement can help to identify degrees of freedom contributing to the ground-state. Also, analysing the deviations from the infinite system can provide a deep understanding of the role of symmetries in connecting effective correlation lengths to produce states and phases of the thermodynamical limit.

Our results for  $\langle S_j \rangle(L, n = 1, U, \Theta^*)$  as a function of the coupling  $U/t$  for finite chains under  $\Theta^*$  are presented in figures 7 and 8. In panels (a), the entanglement entropy for the infinite Hubbard model - calculated from eq. (19) - is represented by a solid black line, whereas  $\langle S_j \rangle(L, n = 1, U, \Theta^*)$  calculated for  $L = 3, 4, 5, 6, 7, 8$  is shown in colored lines and markers. We note that  $\langle S_j \rangle$  is lower than its value in the infinite Hubbard model for  $L$  odd in all coupling regimes, while for even  $L$  it stays within the limits  $1 \leq S_j(L \rightarrow \infty) \leq 2$ . The reason for that is that at half-filling, chains with odd number of sites are magnetized with total spin  $S = 1/2$ , so that  $\lambda_\uparrow > \lambda_\downarrow$  for  $U \gg 1$ . In the extreme,  $U/t \rightarrow \infty$  the Néel state is described by two components with weights corresponding to  $\lambda_\uparrow$  and  $\lambda_\downarrow$ . For closed chains with odd  $L$ , the antiferromagnetic state arising in the limit  $U/t \gg 100$  offers an example of magnetic frustration, absent for even  $L$  as spins  $\uparrow$ 's match consecutive  $\downarrow$ 's.

For the deviations in the average single-site entanglement, we work with the percentual difference  $\langle \delta S_j \rangle$  between the Bethe Ansatz estimate  $\langle S_j \rangle^{BA}(n = 1, U)$  and the calculated  $\langle S_j \rangle(L, n = 1, U, \Theta)$  for finite chains. Explicitly,

$$\langle \delta S_j \rangle(L, n = 1, U, \Theta) = \frac{|\langle S_j \rangle(L, n = 1, U, \Theta) - \langle S_j \rangle^{BA}|}{\langle S_j \rangle^{BA}}. \quad (41)$$

Panel (b) of figures 7 and 8 display  $\langle \delta S_j \rangle$  as a function of  $U/t$  for chains with  $L = 3, 5, 7$  and  $L = 4, 6, 8$  in

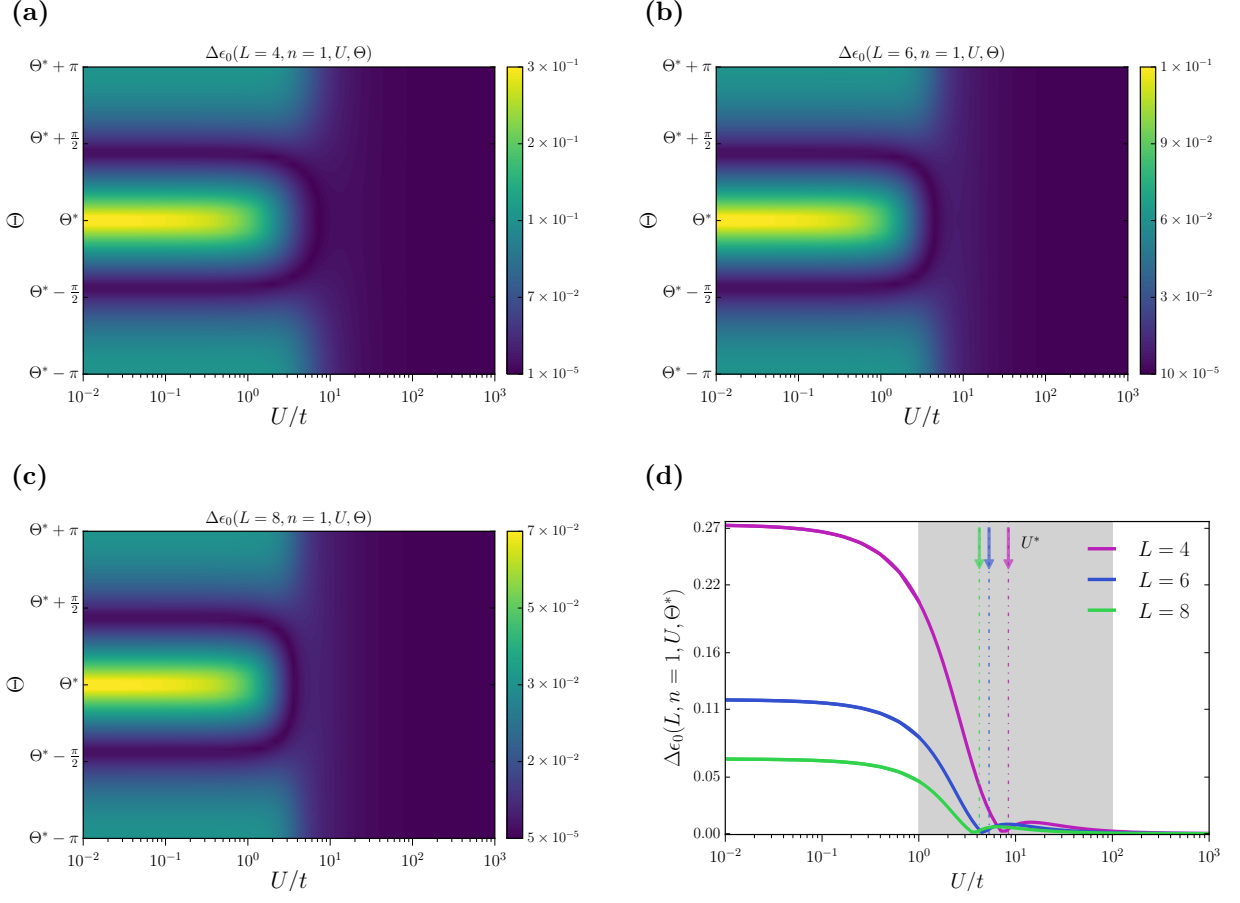


Figure 6. Deviations in the per-site ground-state density energies  $\epsilon_0(L, n = 1, U, \Theta)$  of finite Hubbard chains from the thermodynamical limit  $\epsilon_0^{BA}(n = 1, U)$  calculated from the Bethe Ansatz. Panels (a), (b) and (c) show  $\Delta\epsilon_0(L, n = 1, U, \Theta)$  as a function of the torsion  $\Theta$  and the coupling  $U/t$  for lattices with  $L = 4, 6$  and  $8$ , respectively. Panel (d) displays  $\Delta\epsilon_0(L, n = 1, U, \Theta^*)$  under the special torsion  $\Theta_{\text{even}}^* = \pi$ . The highest deviations from the thermodynamical limit  $L \rightarrow \infty$  are found in the non-interacting and intermediate coupling regimes ( $U/t < 10$ ).

the case where the torsion is  $\Theta^*$ . Similarly to the ground-state energy, chains with odd and even number of sites present opposite trends under  $\Theta^*$ . The behavior of  $\langle \delta S_j \rangle(L, n = 1, U, \Theta)$  is particularly interesting within the shaded region ( $1 \leq U/t \leq 100$ ). For  $L$  odd, the deviation  $\langle \delta S_j \rangle$  is nearly constant for  $U/t \leq 1$  and  $U/t \geq 10$ . The cases  $L = 4, 6, 8$  depict a different trend, the differences in  $\langle S_j \rangle$  start increasing in couplings of one order below those with successive  $L$  even, reaching a maximum value for all even sizes around  $U/t \approx 2.5$  and smoothly decreasing to valleys in  $U/t \approx 6.5, 8.5$  and  $14.5$  for  $L = 4, 6$  and  $8$ , respectively. The couplings  $U/t$  for which  $\langle \delta S_j \rangle$  is minimum are marked in colored arrows on the top of the panels 7 (b) and 8 (b). Following the increasing in the chain size, we observe  $U/t$  to decrease, suggesting not only a scale property, but also the existence of a critical coupling for which a finite system with size  $L$  is able to reproduce with arbitrarily good precision the correlations of the thermodynamical limit. A deep understanding of such property requires further examination; we suggest to investigate other correlation measures, such as the spin correlations and block-block entanglement.

Finally, we analyse the scaling on the ground-state and the average single-site entanglement under  $\Theta^*$ . Figure 9 shows  $\epsilon_0(L, n = 1, U, \Theta^*)$  (a) and  $\langle S_j \rangle(L, n = 1, U, \Theta^*)$  (b) as a function of  $L$  for some values of  $U/t$  ranging from the free (dark blue) to the strongly coupling (yellow) regime. Colored arrows on the right side of the panels indicate the values of  $\epsilon_0(U, n = 1)$  and  $\langle S_j \rangle(U, n = 1)$  for  $L \rightarrow \infty$ . Colored circles and empty squares identify odd and even chains, respectively. Comparing chains with odd and even number of sites, we note the first perform better in low and intermediate coupling regimes. For  $U/t > 1$ , they become comparable, and for  $U/t > 10$ , there is an inversion, as values for even  $L$  are closer to the Bethe Ansatz. The same trend is observed for both ground-state energy and single-site entanglement.

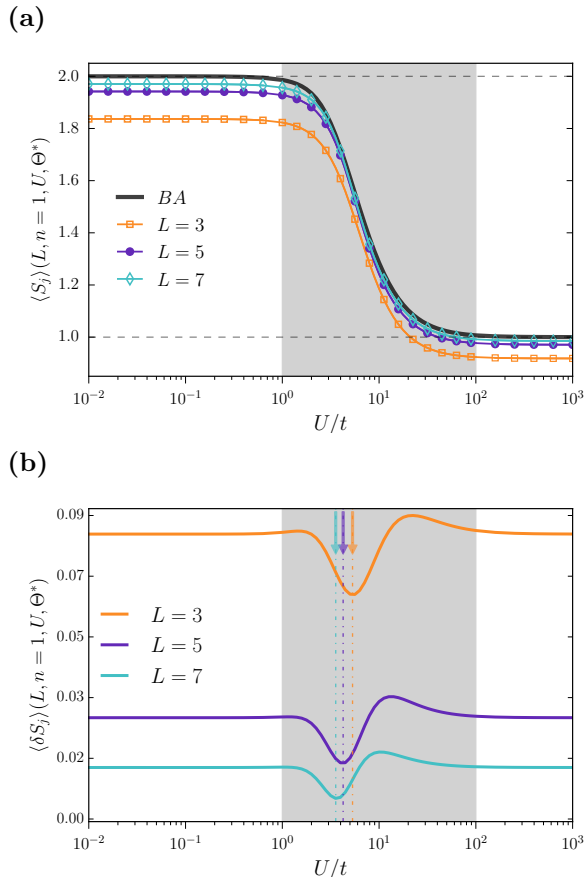


Figure 7. Mean single site entanglement  $\langle S_j \rangle$  as a function of the coupling  $U/t$  for chains with odd number of sites under torsion  $\Theta^*$ . **(a)** The estimate for  $\langle S_j \rangle$  in the limit  $L \rightarrow \infty$  obtained via Bethe Ansatz is represented in black solid lines and colored marked curves show  $\langle S_j \rangle(L, n = 1, U, \Theta^*)$  for chains of odd number of sites  $L = 3, 5, 7$ . **(b)** Percentual difference  $\langle \delta S_j \rangle(L, n = 1, U, \Theta^*)$  from the thermodynamical limit as a function of  $U/t$ . Colored arrows on the top of the right panel indicates the scaled couplings  $U/t$  for which the relative deviations  $\langle \delta S_j \rangle$  are minimum.

## V. CONCLUSIONS

We have discussed the one-dimensional finite Hubbard Hamiltonian under twisted boundary conditions and examined two important invariances present in the infinite model, namely, particle-hole symmetry and momentum conservation. We have derived the special torsion phase which restores these symmetries in finite Hubbard chains by means of local twisted hoppings with phases of  $\Theta_{\text{odd}}^* = \pi/2$  and  $\Theta_{\text{even}}^* = \pi$ . We have presented exact numerical results for the ground-state energy of half-filled chains as a function of the torsion  $\Theta$  and the coupling  $U/t$ , investigating how far from the thermodynamical limit these quantities are for chains with size  $L = 3, 4, 5, 6, 7, 8$  under the special torsion. We show that, ensuring particle-hole and translation symmetry by fixing  $\Theta^*$ , the deviations in the per-site ground-state energy of lattices of few sites ( $L = 7$  or  $L = 8$ ) from the Bethe Ansatz calculation for  $L \rightarrow \infty$  are maximum in small and intermediate coupling regimes, whereas reproduces quite well the insulating phase of the infinite Hubbard model. The analysis of the average single-site entanglement completed our analysis of the phase transition in finite Hubbard lattices and of its scaling behavior. We have identified couplings for which finite lattices enter in the Néel antiferromagnetic insulating phase. Finally, we discussed the differences between chains with even and odd number of sites. Our findings provide new insights into the understanding of scaling laws in phase transitions occurring in finite systems. In particular, examining the role of symmetries in finite chains and their correspondence with the thermodynamical limit can help us to identify the quantum states yielding the most important contributions to the  $L \rightarrow \infty$  limit. Special attention to such states may help us to define novel renormalization-group transformations. Moreover, the understanding of symmetries preservation in few particle systems has a practical importance for quantum technologies, as it can guide the development of protocols for manipulating properties in qubits systems.

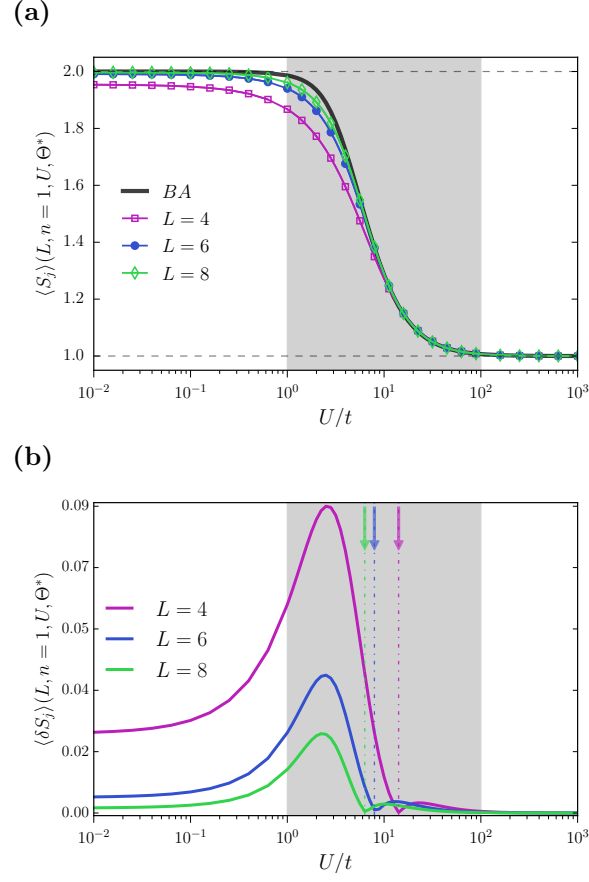


Figure 8. Mean single site entanglement  $\langle S_j \rangle$  as a function of the coupling  $U/t$  for chains with even number of sites under torsion  $\Theta^*$ . **(a)** The estimate for  $\langle S_j \rangle$  in the limit  $L \rightarrow \infty$  obtained via Bethe Ansatz is represented in black solid lines and colored marked curves show  $\langle S_j \rangle(L, n = 1, U, \Theta^*)$  for chains of odd number of sites  $L = 4, 6, 8$ . **(b)** Percentual difference  $\langle \delta S_j \rangle(L, n = 1, U, \Theta^*)$  from the thermodynamical limit as a function of  $U/t$ . Colored arrows on the top of the right panel indicates the scaled couplings  $U/t$  for which the relative deviations  $\langle \delta S_j \rangle$  are minimum.

### ACKNOWLEDGMENTS

LNO acknowledges FAPESP (Fellowship grant no. 12/02702-0) and CNPq (grants no. 312658/2013-3) for financial support. KZ acknowledges support from CNPq (PhD Scholarship grant no. 140703/2014-4) and CAPES (PDSE grant no. 88881.135185/2016-01). ID acknowledges support from the Royal Society through the Newton Advanced Fellowship scheme (grant no. NA140436) and CNPq through the PVE scheme (grant no. 401414/2014-0).

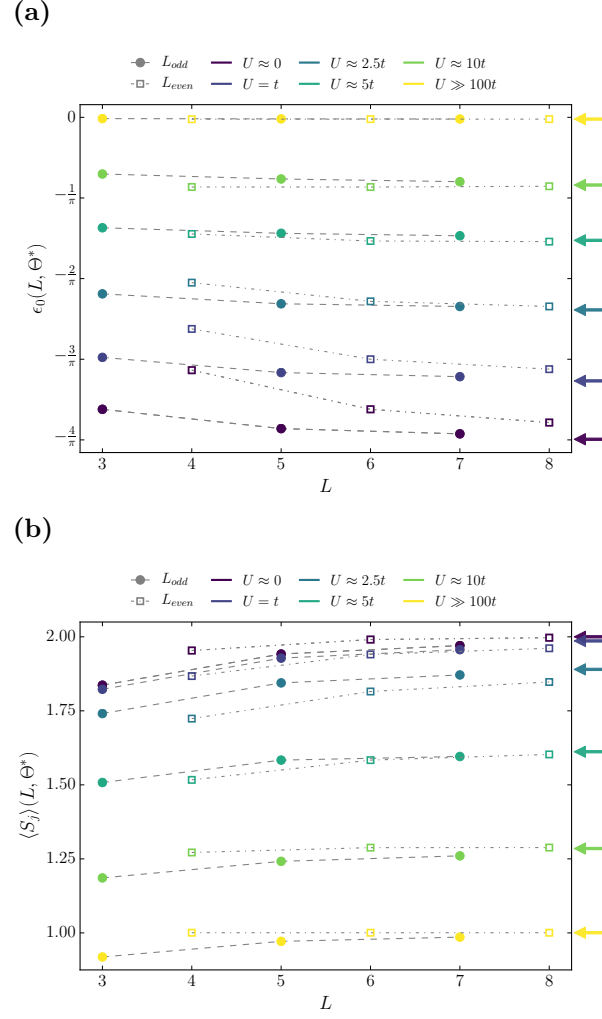


Figure 9. Scaling of the ground-state energy (a) and average single-site entanglement (b) under twisted boundary conditions with torsion  $\Theta^*$  for various coupling regimes. Empty squares represent  $L$  even and filled circles correspond to  $L$  odd. The different scaling trend followed by  $L$  even (dot-dashed lines) and odd (dashed lines) is understood in terms of the degeneracy of spin configurations contributing to the ground-state in the case of  $L$  even under  $\Theta^*$ . The degeneracy under particle-hole symmetry for  $L$  even reduces the number of effective states needed to represent the thermodynamical limit. Values of  $\epsilon_0^{BA}(n=1, U)$  and  $\langle S_j \rangle^{BA}(n=1, U)$  in the thermodynamical limit ( $L \rightarrow \infty$ ) are indicated by colored arrows on the right side of the axis. .

- 
- <sup>1</sup> R. Jordens, N. Strohmaier, K. Günter, H. Moritz, and T. Esslinger, *Nature* **455**, 204 (2008).
  - <sup>2</sup> T. Byrnes, N. Y. Kim, K. Kusudo, and Y. Yamamoto, *Physical Review B* **78**, 075320 (2008).
  - <sup>3</sup> J. Salfi, J. A. Mol, R. Rahman, G. Klimeck, M. Y. Simmons, L. C. L. Hollenberg, and S. Rogge, *Nature Communications* **7**, 11342 (2016).
  - <sup>4</sup> S. Baier, M. J. Mark, D. Petter, K. Aikawa, L. Chomaz, Z. Cai, M. Baranov, P. Zoller, and F. Ferlaino, *Science* **352**, 201 (2016).
  - <sup>5</sup> G. J. A. Edge, R. Anderson, D. Jervis, D. C. McKay, R. Day, S. Trotzky, and J. H. Thywissen, *Physical Review A* **92**, 063406 (2015).
  - <sup>6</sup> M. F. Parsons, A. Mazurenko, C. S. Chiu, G. Ji, D. Greif, and M. Greiner, *Science* **353**, 1253 (2016).
  - <sup>7</sup> M. Boll, T. A. Hilker, G. Salomon, A. Omran, J. Nespolo, L. Pollet, I. Bloch, and C. Gross, *Science* **353**, 1257 (2016).
  - <sup>8</sup> G. Vidal, J. I. Latorre, E. Rico, and A. Kitaev, *Physical Review Letters* **90**, 227902 (2003).
  - <sup>9</sup> L. Amico, R. Fazio, A. Osterloh, and V. Vedral, *Reviews of Modern Physics* **80**, 517 (2008).



- <sup>10</sup> N. Laflorencie, *Physics Reports* **646**, 1 (2016), quantum entanglement in condensed matter systems.
- <sup>11</sup> J. T. Gammel, D. Campbell, and E. Y. Loh, *Synthetic Metals* **57**, 4437 (1993).
- <sup>12</sup> P. Papanastasiou, C. Ottaviani, and S. Pirandola, *Physical Review A* **96**, 042332 (2017).
- <sup>13</sup> M. Kormos, M. Collura, G. Takács, and P. Calabrese, *Nature Physics* **13**, 246 (2017).
- <sup>14</sup> B. Wang, F. N. Ünal, and A. Eckardt, arXiv preprint arXiv:1802.06815 (2018).
- <sup>15</sup> P. R. C. Kent, R. Q. Hood, A. J. Williamson, R. J. Needs, W. M. C. Foulkes, and G. Rajagopal, *Phys. Rev. B* **59**, 1917 (1999).
- <sup>16</sup> C. Gros, *Physical Review B* **53**, 6865 (1996).
- <sup>17</sup> C. Lin, F. H. Zong, and D. M. Ceperley, *Phys. Rev. E* **64**, 016702 (2001).
- <sup>18</sup> M. Dagrada, S. Karakuzu, V. L. Vildosola, M. Casula, and S. Sorella, *Phys. Rev. B* **94**, 245108 (2016).
- <sup>19</sup> J. Cirac, D. Pérez-García, N. Schuch, and F. Verstraete, *Annals of Physics* **378**, 100 (2017).
- <sup>20</sup> S. Yang, Z.-C. Gu, and X.-G. Wen, *Physical Review Letters* **118**, 110504 (2017).
- <sup>21</sup> K. Zawadzki, I. D'Amico, and L. N. Oliveira, *Brazilian Journal of Physics* **47**, 488 (2017).
- <sup>22</sup> J. Hubbard, *Proceedings of the Royal Society of London A: Mathematical, Physical and Engineering Sciences* **276**, 238 (1963).
- <sup>23</sup> E. H. Lieb and F. Wu, *Physica A: Statistical Mechanics and its Applications* **321**, 1 (2003), statphys-Taiwan-2002: Lattice Models and Complex Systems.
- <sup>24</sup> B. S. Shastri and B. Sutherland, *Physical Review Letters* **65**, 243 (1990).
- <sup>25</sup> F. C. Alcaraz, M. N. Barber, and M. T. Batchelor, *Annals of Physics* **182**, 280 (1988).
- <sup>26</sup> M. Shiroishi and M. Wadati, *Journal of the Physical Society of Japan* **66**, 2288 (1997).
- <sup>27</sup> R. Yue and T. Deguchi, *Journal of Physics A: Mathematical and General* **30**, 849 (1997).
- <sup>28</sup> T. Fukui and N. Kawakami, *Phys. Rev. B* **58**, 16051 (1998).
- <sup>29</sup> M. Rigol, *Phys. Rev. Lett.* **103**, 100403 (2009).
- <sup>30</sup> P. Weinberg, M. Bukov, L. D'Alessio, A. Polkovnikov, S. Vajna, and M. Kolodrubetz, *Physics Reports* **688**, 1 (2017), adiabatic Perturbation Theory and Geometry of Periodically-Driven Systems.
- <sup>31</sup> R. N. Bannister and N. d'Ambrumenil, *Phys. Rev. B* **61**, 4651 (2000).
- <sup>32</sup> We note that phases  $0 \leq \Theta \leq \pi$  are symmetric to those from  $2\pi$  to  $\pi$  with the first half of trigonometric circle by  $\Theta \rightarrow 2\pi - \Theta$ .
- <sup>33</sup> S.-J. Gu, S.-S. Deng, Y.-Q. Li, and H.-Q. Lin, *Phys. Rev. Lett.* **93**, 086402 (2004).
- <sup>34</sup> D. Larsson and H. Johannesson, *Phys. Rev. Lett.* **95**, 196406 (2005).
- <sup>35</sup> V. V. Franca and K. Capelle, *Physical Review Letters* **100**, 070403 (2008).
- <sup>36</sup> H. Q. Lin, *Phys. Rev. B* **42**, 6561 (1990).
- <sup>37</sup> H. Lin, J. Gubernatis, H. Gould, and J. Tobochnik, *Computers in Physics* **7**, 400 (1993), <https://aip.scitation.org/doi/pdf/10.1063/1.4823192>.
- <sup>38</sup> E. R. Gagliano, E. Dagotto, A. Moreo, and F. C. Alcaraz, *Phys. Rev. B* **34**, 1677 (1986).
- <sup>39</sup> A. Osterloh, L. Amico, G. Falci, and R. Fazio, *Nature* **416**, 608 (2002).
- <sup>40</sup> L.-A. Wu, M. S. Sarandy, D. A. Lidar, and L. J. Sham, *Phys. Rev. A* **74**, 052335 (2006).
- <sup>41</sup> J. Vidal, G. Palacios, and R. Mosseri, *Phys. Rev. A* **69**, 022107 (2004).
- <sup>42</sup> D. Larsson and H. Johannesson, *Phys. Rev. A* **73**, 042320 (2006).

### Appendix A: Single-site entanglement deviations as a function of $\Theta$ and $U/t$

In section IV, we presented results (Figs. 7 and 8) for the deviations  $\delta S_j$  from the thermodynamical limit in the single-site entanglement of finite Hubbard chains under the special torsion  $\Theta^*$ . Here, we present the results for  $\delta S_j$  as a function of the torsion  $\Theta$  and the coupling  $U/t$ .

Figure 10 shows the deviations in the average single-site entanglement for chains with an odd number of sites  $L = 3, 5$  and  $7$ . Similarly to the periodic behavior with respect to  $\Theta$  observed in the plots for the ground-state energy  $\Delta\epsilon_0(L, n = 1, U, \Theta)$ , the deviations  $\delta S_j(L, n = 1, U, \Theta)$  for odd  $L$  are minima under the special torsion  $\Theta^*$  and maxima at the points  $\Theta^* \pm \pi/2$ . For odd  $L$ , the deviations are constant in small and strong coupling regimes; for intermediate coupling regimes  $1 < U/t < 10$ , a complex structure arises.

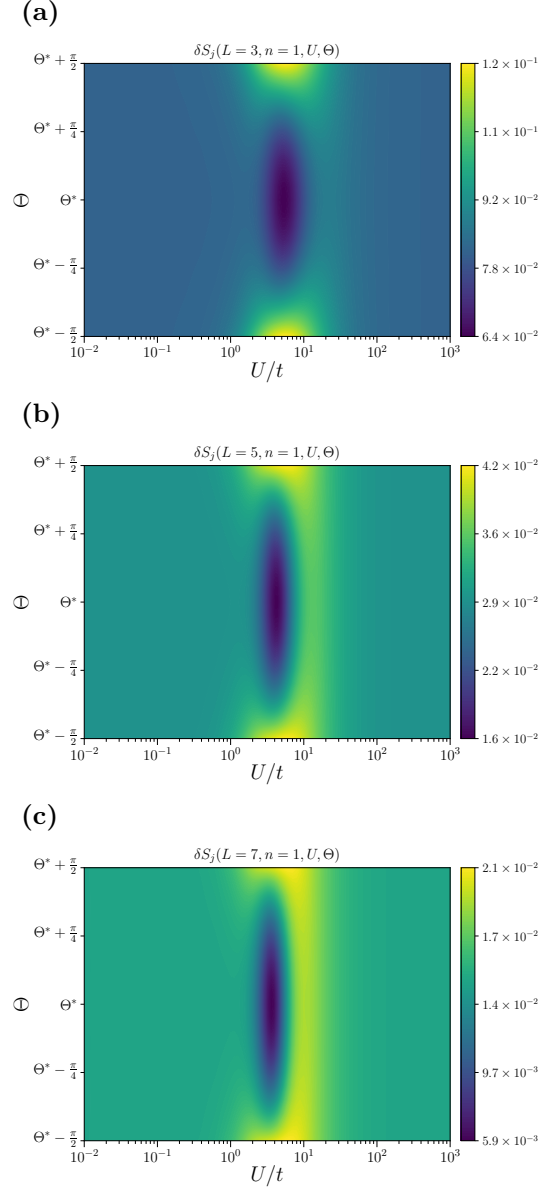


Figure 10. Deviations in the average single-site entanglement  $\langle S_j \rangle(L, n = 1, U, \Theta)$  of finite Hubbard chains from the thermodynamical limit  $\langle S_j \rangle^{BA}(n = 1, U)$  calculated from the Bethe Ansatz. Panels (a), (b) and (c) show  $\delta S_j(L, n = 1, U, \Theta)$  as a function of the torsion  $\Theta$  and the coupling  $U/t$  for lattices with  $L = 3, 5$  and  $7$ , respectively. The lowest deviations from the thermodynamical limit  $L \rightarrow \infty$  are found in the intermediate coupling regimes ( $1 < U/t < 10$ ), the minimum deviation occurring under  $\Theta^*$ .

The percentual deviations from the Bethe Ansatz in the case of chains with even number of sites is shown in figure 11. The deviation is below  $10^{-8}$  in small and strong coupling regimes, being amplified for couplings  $1 < U/t < 10$  specially at the torsion  $\Theta^*$  ensuring particle-hole symmetry.

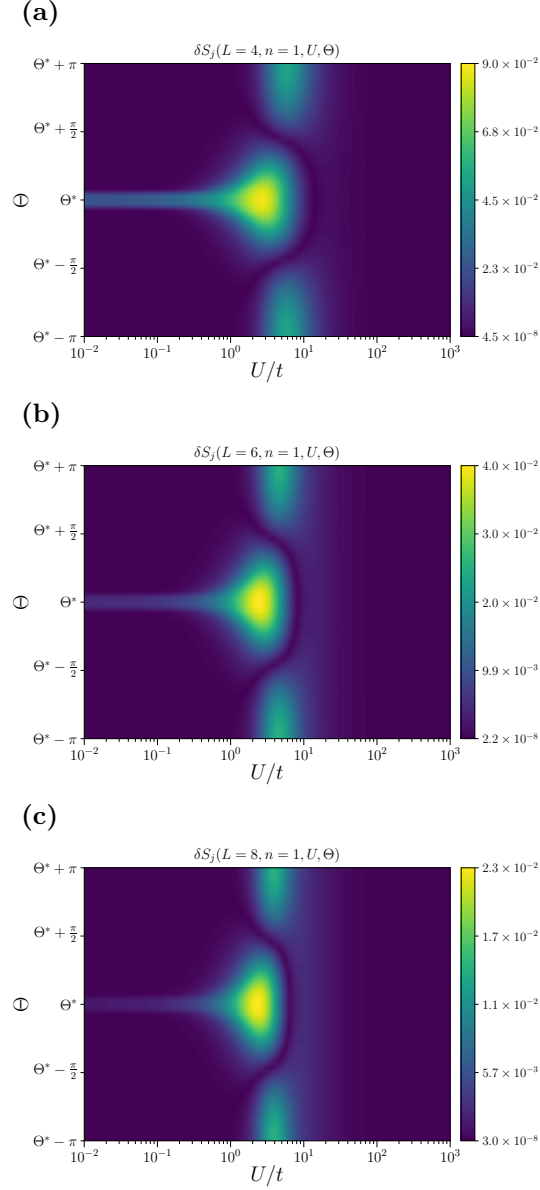


Figure 11. Deviations in the average single-site entanglement  $\langle S_j \rangle(L, n = 1, U, \Theta)$  of finite Hubbard chains from the thermodynamical limit  $\langle S_j \rangle^{BA}(n = 1, U)$  calculated from the Bethe Ansatz. Panels (a), (b) and (c) show  $\delta S_j(L, n = 1, U, \Theta)$  as a function of the torsion  $\Theta$  and the coupling  $U/t$  for lattices with  $L = 4, 6$  and  $8$ , respectively. The highest deviations from the thermodynamical limit  $L \rightarrow \infty$  are found in the intermediate coupling regimes ( $1 < U/t < 10$ ), the maximum deviation occurring under  $\Theta^*$ .

### Appendix B: Case study: trimer

For instance, consider a trimer  $L = 3$  with  $\mu = 0$ . For open and periodic boundary conditions, Hamiltonian of eq. (1) can be written as

$$\begin{aligned} \hat{H}_{OBC}(L = 3) = & -t(\hat{c}_{1\sigma}^\dagger \hat{c}_{2\sigma} + \hat{c}_{2\sigma}^\dagger \hat{c}_{1\sigma}) - t(\hat{c}_{2\sigma}^\dagger \hat{c}_{3\sigma} + \hat{c}_{3\sigma}^\dagger \hat{c}_{2\sigma}) \\ & + U\hat{n}_{1\uparrow}\hat{n}_{1\downarrow} + U\hat{n}_{2\uparrow}\hat{n}_{2\downarrow} + U\hat{n}_{3\uparrow}\hat{n}_{3\downarrow} \end{aligned} \quad (\text{B1})$$

and

$$\hat{H}_{PBC}(L = 3) = \hat{H}_{OBC}(L = 3) - t(\hat{c}_{1\sigma}^\dagger \hat{c}_{3\sigma} + \hat{c}_{3\sigma}^\dagger \hat{c}_{1\sigma}), \quad (\text{B2})$$

respectively.

For twisted boundary conditions with twist phase  $\theta$  we replace  $\hat{c}_\ell^\dagger \rightarrow e^{i\theta\ell} \hat{c}_\ell^\dagger$  to write the Hamiltonian (1) as

$$\begin{aligned} \hat{H}_{TBC}(L = 3) = & -te^{-i\theta}(\hat{c}_1^\dagger \hat{c}_2 + \hat{c}_2^\dagger \hat{c}_3 + \hat{c}_3^\dagger \hat{c}_1) \\ & -te^{i\theta}(\hat{c}_2^\dagger \hat{c}_1 + \hat{c}_3^\dagger \hat{c}_2 + \hat{c}_1^\dagger \hat{c}_3) \\ & + U\hat{n}_{1\uparrow}\hat{n}_{1\downarrow} + U\hat{n}_{2\uparrow}\hat{n}_{2\downarrow} + U\hat{n}_{3\uparrow}\hat{n}_{3\downarrow}. \end{aligned} \quad (\text{B3})$$

At half-filling the basis set comprises 18 states, 9 associated with  $z$  component of spin  $S_z = -1/2$  and 9 with  $S_z = +1/2$ , which are degenerate. They are:

$$\begin{aligned} |L = 3, S = 1/2, S_z = 1/2, b = 1\rangle &= \hat{c}_{2\uparrow}^\dagger \hat{c}_{3\uparrow}^\dagger \hat{c}_{3\downarrow}^\dagger |0\rangle \\ |L = 3, S = 1/2, S_z = 1/2, b = 2\rangle &= \hat{c}_{2\uparrow}^\dagger \hat{c}_{2\downarrow}^\dagger \hat{c}_{3\uparrow}^\dagger |0\rangle \\ |L = 3, S = 1/2, S_z = 1/2, b = 3\rangle &= \hat{c}_{1\downarrow}^\dagger \hat{c}_{2\uparrow}^\dagger \hat{c}_{3\uparrow}^\dagger |0\rangle \\ |L = 3, S = 1/2, S_z = 1/2, b = 4\rangle &= \hat{c}_{1\uparrow}^\dagger \hat{c}_{3\uparrow}^\dagger \hat{c}_{3\downarrow}^\dagger |0\rangle \\ |L = 3, S = 1/2, S_z = 1/2, b = 5\rangle &= \hat{c}_{1\uparrow}^\dagger \hat{c}_{2\downarrow}^\dagger \hat{c}_{3\uparrow}^\dagger |0\rangle \\ |L = 3, S = 1/2, S_z = 1/2, b = 6\rangle &= \hat{c}_{1\uparrow}^\dagger \hat{c}_{2\uparrow}^\dagger \hat{c}_{3\downarrow}^\dagger |0\rangle \\ |L = 3, S = 1/2, S_z = 1/2, b = 7\rangle &= \hat{c}_{1\uparrow}^\dagger \hat{c}_{2\uparrow}^\dagger \hat{c}_{2\downarrow}^\dagger |0\rangle \\ |L = 3, S = 1/2, S_z = 1/2, b = 8\rangle &= \hat{c}_{1\uparrow}^\dagger \hat{c}_{1\downarrow}^\dagger \hat{c}_{3\uparrow}^\dagger |0\rangle \\ |L = 3, S = 1/2, S_z = 1/2, b = 9\rangle &= \hat{c}_{1\uparrow}^\dagger \hat{c}_{1\downarrow}^\dagger \hat{c}_{2\uparrow}^\dagger |0\rangle. \end{aligned} \quad (\text{B4})$$

Projecting the operator  $\hat{H}$  in eq. (B3) into the basis defined by eq. (B4), we obtain the corresponding matrix Hamiltonian

$$H_{L=3}(\theta) = t \begin{pmatrix} 0 & 0 & 0 & -e^{-i\theta} & 0 & e^{i\theta} & 0 & e^{-i\theta} & -e^{i\theta} \\ 0 & 0 & 0 & 0 & e^{i\theta} & -e^{i\theta} & e^{-i\theta} & -e^{-i\theta} & 0 \\ 0 & 0 & 0 & e^{-i\theta} & -e^{i\theta} & 0 & -e^{-i\theta} & 0 & e^{i\theta} \\ -e^{i\theta} & 0 & e^{i\theta} & \tilde{U} & e^{-i\theta} & -e^{-i\theta} & 0 & 0 & 0 \\ 0 & e^{-i\theta} & -e^{-i\theta} & e^{i\theta} & \tilde{U} & 0 & 0 & -e^{i\theta} & 0 \\ e^{-i\theta} & -e^{-i\theta} & 0 & -e^{i\theta} & 0 & \tilde{U} & e^{i\theta} & 0 & 0 \\ 0 & e^{i\theta} & -e^{i\theta} & 0 & 0 & e^{-i\theta} & \tilde{U} & 0 & -e^{-i\theta} \\ e^{i\theta} & -e^{i\theta} & 0 & 0 & -e^{-i\theta} & 0 & 0 & \tilde{U} & e^{-i\theta} \\ -e^{-i\theta} & 0 & e^{-i\theta} & 0 & 0 & 0 & -e^{i\theta} & e^{i\theta} & \tilde{U} \end{pmatrix}, \quad (\text{B5})$$

where  $\tilde{U} = U/t$ .

Notice that, the periodic boundary condition, can be recovered by choosing  $\theta = 0$ . As discussed in sec. II,  $\theta = \pi/2$  ensures particle-hole symmetry.

In the non-interacting case,  $U = 0$  with  $\theta = \pi/2$  the ground-state is a combination of three states

$$|\Psi_0\rangle = \frac{1}{\sqrt{3}} |\psi_0\rangle + \frac{1+i\sqrt{3}}{2\sqrt{3}} |\psi_1\rangle - \frac{1-i\sqrt{3}}{2\sqrt{3}} |\psi_2\rangle, \quad (\text{B6})$$

where

$$\begin{aligned}
|\psi_0\rangle &= \frac{1}{\sqrt{3}}(|\uparrow\uparrow\downarrow\rangle + |\uparrow\downarrow-\uparrow\rangle - |\downarrow\uparrow\uparrow\rangle) \\
|\psi_1\rangle &= \frac{1}{\sqrt{3}}(-|\uparrow\downarrow\uparrow\rangle + |\uparrow\downarrow\uparrow-\downarrow\rangle - |\downarrow\uparrow\uparrow\rangle) \\
|\psi_2\rangle &= \frac{1}{\sqrt{3}}(|\downarrow\uparrow\uparrow\rangle + |\uparrow\uparrow\downarrow-\downarrow\rangle - |\uparrow-\uparrow\downarrow\rangle).
\end{aligned} \tag{B7}$$

In order to calculate the single-site entanglement, we must compute the reduced density matrix by tracing the degrees of freedom of two sites, i.e.,

$$\rho^k = \text{Tr}_{\ell \neq k} |\Psi_0\rangle \langle \Psi_0|, \tag{B8}$$

where  $i, j, k$  refers to the sites labels.

On basis of  $|\psi\rangle$ 's the density matrix is

$$\rho = \begin{pmatrix} \frac{1}{3} & \frac{1+i\sqrt{3}}{6} & -\frac{1-i\sqrt{3}}{6} \\ \frac{1-i\sqrt{3}}{6} & \frac{1}{3} & \frac{1+i\sqrt{3}}{6} \\ -\frac{1+i\sqrt{3}}{6} & \frac{1-i\sqrt{3}}{6} & \frac{1}{3} \end{pmatrix}. \tag{B9}$$

Let's first consider the trace over sites 0 and 1:

$$\begin{aligned}
\rho_2 &= \text{Tr}_{0,1} [\rho] \\
&= \sum_{\sigma_0, \sigma_1} \langle \sigma_0 \sigma_1 | \rho^+ | \sigma_0 \sigma_1 \rangle,
\end{aligned} \tag{B10}$$

where  $\sigma = \uparrow, \downarrow$ .

$$\rho_2 = \text{Tr}_{1,3} [\rho]. \tag{B11}$$

The reduced density matrix is diagonal since the products of states of sites 0 and 1 with each  $|\Psi\rangle$  are

$$\begin{aligned}
\langle \sigma_0 \sigma_1 | \psi_0 &= \frac{1}{\sqrt{3}} \left[ \delta_{\sigma_0, \uparrow} \delta_{\sigma_1, \uparrow} |\downarrow\rangle + \delta_{\sigma_0, \uparrow} \delta_{\sigma_1, -} |\uparrow\rangle - \delta_{\sigma_0, -} \delta_{\sigma_1, \uparrow} |\uparrow\rangle \right] \\
\langle \sigma_0 \sigma_1 | \psi_1 &= \frac{1}{\sqrt{3}} \left[ -\delta_{\sigma_0, \uparrow} \delta_{\sigma_1, \downarrow} |\uparrow\rangle + \delta_{\sigma_0, \uparrow} \delta_{\sigma_1, \uparrow} |\downarrow\rangle - \delta_{\sigma_0, -} \delta_{\sigma_1, \uparrow} |\uparrow\rangle \right] \\
\langle \sigma_0 \sigma_1 | \psi_2 &= \frac{1}{\sqrt{3}} \left[ \delta_{\sigma_0, \downarrow} \delta_{\sigma_1, \uparrow} |\uparrow\rangle + \delta_{\sigma_0, \uparrow} \delta_{\sigma_1, \uparrow} |\downarrow\rangle - \delta_{\sigma_0, \uparrow} \delta_{\sigma_1, -} |\uparrow\rangle \right],
\end{aligned} \tag{B12}$$

yielding

$$\rho_2 = \frac{1}{3} \begin{pmatrix} |\alpha_1|^2 + |\alpha_2|^2 & 0 & 0 & 0 \\ 0 & |\alpha_0|^2 & 0 & 0 \\ 0 & 0 & 2|\alpha_0|^2 + |\alpha_1|^2 + |\alpha_2|^2 & 0 \\ 0 & 0 & 0 & |\alpha_1|^2 + |\alpha_2|^2 \end{pmatrix}, \tag{B13}$$

where

$$\begin{aligned}
\alpha_0 &= \frac{1}{\sqrt{3}} \rightarrow |\alpha_0|^2 = \frac{1}{3} \\
\alpha_1 &= \frac{1+i\sqrt{3}}{6} \rightarrow |\alpha_1|^2 = \frac{1}{3} \\
\alpha_2 &= \frac{1-i\sqrt{3}}{6} \rightarrow |\alpha_2|^2 = \frac{1}{3},
\end{aligned} \tag{B14}$$

so that eq. (B15) is expressed as

$$\rho_2 = \begin{pmatrix} \frac{2}{9} & 0 & 0 & 0 \\ 0 & \frac{1}{9} & 0 & 0 \\ 0 & 0 & \frac{4}{9} & 0 \\ 0 & 0 & 0 & \frac{2}{9} \end{pmatrix}. \quad (\text{B15})$$

The mean single-site entanglement is therefore

$$\begin{aligned} S_2(U = 0) &= -\frac{1}{9} \left[ 4 \log\left(\frac{2}{9}\right) + \log\left(\frac{1}{9}\right) + 4 \log\left(\frac{4}{9}\right) \right] \\ &\approx 1.8365. \end{aligned} \quad (\text{B16})$$

The Mott-insulating phase ( $U/t \rightarrow \infty$ ) of the Hubbard trimer is the other limit in which analytical calculations are straightforward. The high price for double occupation reduces the basis set in eq. (B4) to only three components  $|\downarrow\uparrow\uparrow\rangle$ ,  $|\downarrow\uparrow\downarrow\rangle$  and  $|\uparrow\uparrow\downarrow\rangle$ . The probabilities to have empty ( $\lambda_-$ ) and double occupied ( $\lambda_{\uparrow\uparrow}$ ) sites vanishes. Once we fixed the magnetization of the system to be  $m = \frac{1}{3}$ ,  $\lambda_{\uparrow} = \frac{2}{3}$  and  $\lambda_{\downarrow} = \frac{1}{3}$ , so that the single-site entanglement is

$$\begin{aligned} S_2(U \rightarrow \infty) &= -\frac{1}{3} \left[ 2 \log\left(\frac{2}{3}\right) + \log\left(\frac{1}{3}\right) \right] \\ &\approx 0.9183. \end{aligned} \quad (\text{B17})$$